Delle Piane et al., 2018, Generation of amorphous carbon and crystallographic texture during low temperature sub-seismic slip in calcite fault gouge: Geology, https://doi.org/10.1130/G39584.1.

This file includes text, figures and tables divided into five Data Repository (DR) items:

1. Image analysis of sheared samples
2. Travertine textural characterization
3. TKD and TEM procedure
4. Calculation of frictional heat rise during shearing
5. EDS and Raman analysis of gouge and identification of amorphous carbon

**Item DR 1: Image Analysis of Sheared Samples**

Detailed microstructural characterization of the deformed blocks was carried out on samples extracted from the highest strained portions of each block (i.e. gouge zones) viewed on surfaces orthogonal to the shear plane (X-Z) and parallel to the transport direction (X). BSE images were collected at magnifications of 10kX, 20kX and 50kX on carbon coated polished thin sections using a Tescan Tima FE-SEM operated at 5 kV and working distance of 10 mm. Quantitative image analysis was conducted using the Fiji platform (Schindelin et al., 2012) to characterize grain size and shape within the gouge (cfr. Marone and Scholz, 1989). Before analysis, the original images were de-noised using a mean filter; the contrast was then improved by normalizing the gray level values of the images. After application of an edge finding algorithm, images were made binary and processed through a series of morphological operations (erode, dilate, open and close). Finally, a watershed algorithm was applied to separate touching particles. Objects in the images were then characterized in terms of their equivalent circular radius (calculated as the square root of the object area divided by π) and circularity (calculated as $4\pi\cdot(\text{area}/\text{perimeter}^2)$). A circularity value of 1.0 indicates a perfect circle. As the value approaches 0.0, it indicates an increasingly elongated polygon.

Image analysis of gouge particles based on SEM images revealed that the resolvable grain size ranges between 10 nm and approximately 5 μm (Figure DR1A). In the range of 0.1- 3.16 μm, the particle size distribution follows a power law relationship of the form:

$$N(S) \approx S^{-D}$$

where $N(S)$ is the number of particles less than size $S$ and $D$ the slope of the best fit line on a log $N(S)$ against log $S$ graph (Figure DR1B). A steep slope (i.e. high D value) signifies a high percentage of very small grains, whereas a shallow slope indicates a low D value and relatively fewer small grains. In our experiments the value of $D$ in the gouge increases with shear displacement from 1.58 at 20 mm to 2.16 at 120 mm of shear (Figure DR-1C). The particles also become more circular as indicated by the circularity parameter, which compares perimeter of a circle (circularity = 1) with that of the grain, increasing from 0.77 at 20 mm to 0.84 at 120 mm of shear (Figure DR1C).

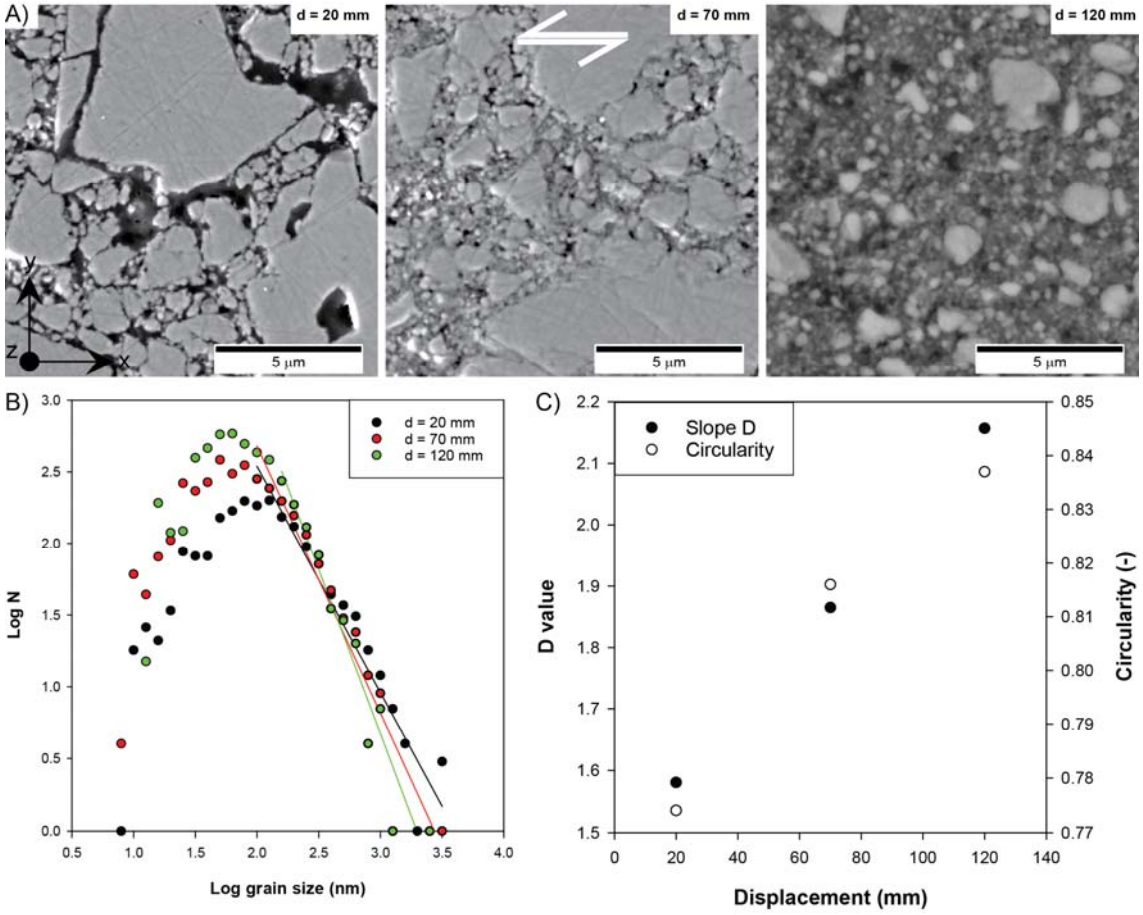


Figure DR1. A) Evolution of microstructure as a function of shear displacement (d) in the Travertine samples used in this study. SEM images of the deformation induced gouge material taken perpendicular to the shear plane in samples sheared to different amount of shear displacement. B) Grain size distribution obtained from image analysis of SEM images acquired from the gouge zone of different samples. N is the number of particles. In the range of 0.1- 3.16 μm, the particle size distribution is well described by a power law with slope D (shown in the figure by the straight black, red and green lines). C) Exponent of the fitted power law grain size distribution (D value) and circularity of the gouge particles derived from image analysis plotted as a function of shear displacement.

**Item DR 2: Travertine Textural Characterization**

Neutron diffraction provides bulk texture measurements averaged over relatively large samples (up to several $cm^3$). Neutron diffraction texture data were collected at the KOWARI diffractometer at the Australian Nuclear Science and Technology Organization (ANSTO). Samples were mounted on an Eulerian cradle, and complete pole figure measurements were achieved through step-wise rotation of the goniometer polar angle ($\chi$) and azimuthal angle ($\varphi$) resulting in approximately 5° × 5° angular mesh. Multiple calcite pole figures corresponding to the diffraction peaks of the (104), (006), (110) and (113) planes were obtained simultaneously utilizing 15° coverage of the KOWARI detector, at a single detector position at $2\theta = 36°$ while using a wavelength of 1.65 Å.

Spatially resolved crystallographic orientation information were collected via EBSD from the X-Z polished blocks used for image analysis. EBSD (e.g. Prior et al., 1999) data were acquired using a TESCAN Mira3 FE-SEM and Oxford Instruments AZTeC software at Curtin University **f**rom a polished thin section cut perpendicular to the shear plane and parallel to the shear direction. Maps were collected at several regions of interest at ~20 mm working distance, sample tilt of 70°, 1 μm step size, and using 20 kV acceleration voltage. EBSD patterns were acquired using 4 x 4 binning and high gain, and indexed using HKL database calcite match units, with up to 8 bands detected at a Hough resolution of 60 and mean angular deviation tolerance of 1°. Processing of EBSD data was done via Oxford Instruments Channel 5.11 and involved removal of isolated, data points in highly misorientated orientations (wildspike correction), followed by up to six nearest neighbor zero solution extrapolation. Grains were defined in the 'Tango' module of Channel 5.11 using an algorithm based on 10° misorientation threshold. Tango was used to identify *e*-twins, which are expressed as lamellar domains with characteristic 78° misorientations around $<20\bar{2}1>$ relative to the host grain. Thematic maps were produced in Tango. Pole figures (lower hemisphere equal area projections) were plotted in the map x-y-z reference frame using the 'Mambo' module of Channel 5.11, and pole figure data were contoured using default settings.

EBSD analysis shows that the intact travertine preserves calcite sparry crystals oriented with c-axes nearly perpendicular to the macroscopic bedding, abundant intra-crystal low-angle boundaries, and almost no twins (Figure DR2B). Subgrain boundaries are parallel to each other with misorientation angles of 3-8°; within individual subgrains, lattice distortions are below 2° over length scales of ~ 100 μm (see profiles at the bottom of Figure DR1). These features are interpreted to represent primary growth with typical 'scale growth' characteristics (Timms et al. 2009). During initial fracturing, large relict clasts close to fractures develop e-twins (Figure DR2C). Within the gouge zone, the grain size was too small to be indexed by conventional EBSD analysis, therefore nanoscale spatial resolution crystallographic and chemical information was acquired by TKD mapping of an ultra-thin, electron transparent foil prepared from a fine grained region of interest in the gouge using focused-ion-beam milling (for location, see Figure DR2D).

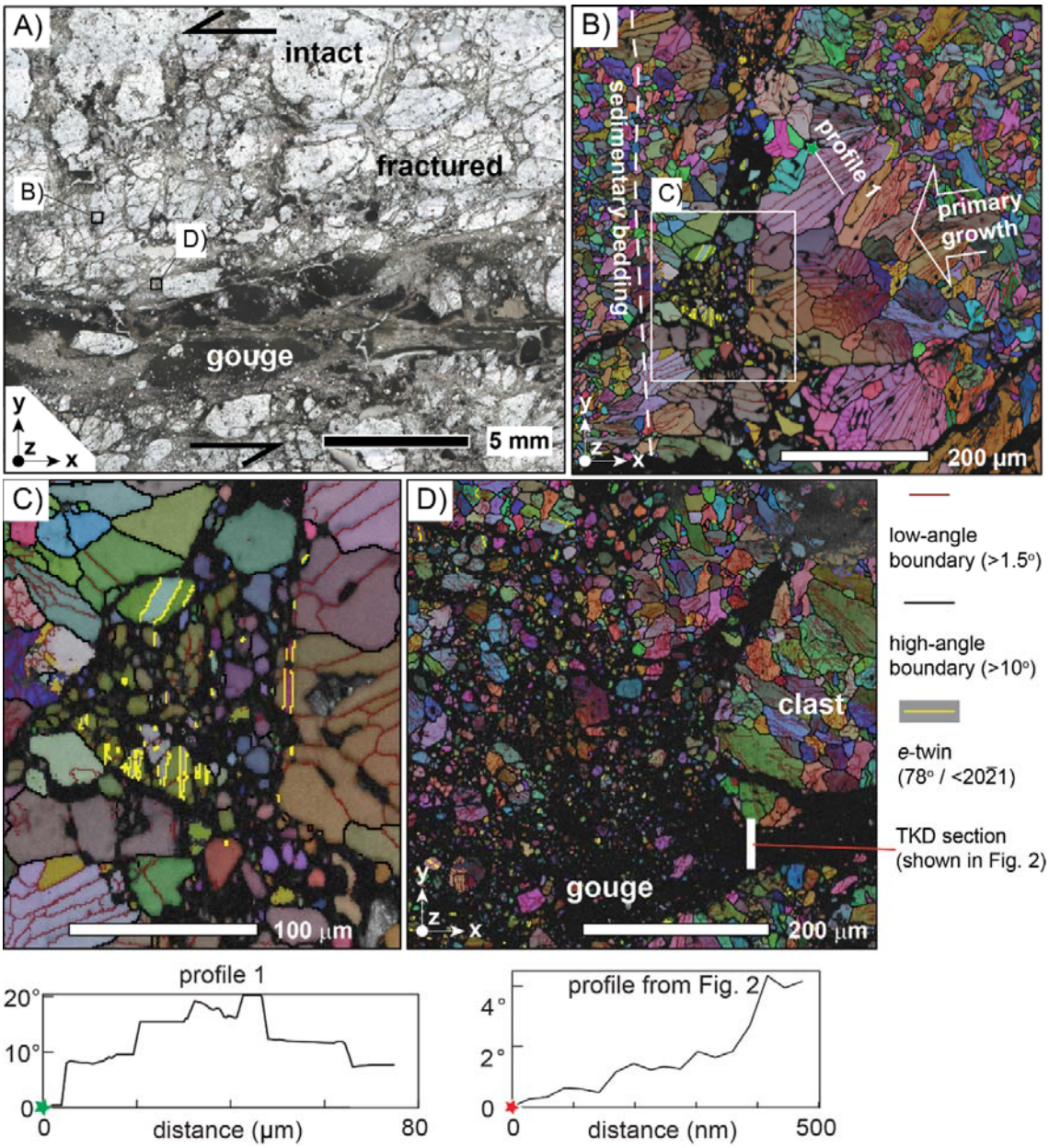


Figure DR2. Characteristic microstructure of the sheared travertine. A) Reflected light optical image of a polished mount extracted from a sample sheared to 120 mm of shear displacement showing intact, fractured and gouge domains. Black squares indicate the position of the EBSD maps shown in B and D. Sedimentary bedding of the travertine is vertical, arrows indicate sense of shear during the experiments. B) EBSD map in all Euler colour scheme with overlain grain boundary map from the fractured domain showing primary growth texture in the intact calcite crystals and grain size reduction and twinning in the fractured area. C) detail view of the fracture area highlighting the presence of *e*-twins expressed as lamellar domains with characteristic 78° mis-orientations around <20$\bar{2}$1> relative to the host grains. D) EBSD map in all Euler colour scheme with overlain grain boundary map from the gouge domain showing grain comminution and large areas of non-indexed regions (in black) also shown is the location of the TKD sections shown in Figure 2 in the main text. Also shown are misorientation profiles related to i) primary growth in calcite sparry crystals (profile 1, location indicated in B) and ii) to of a sub-micron scale calcite grain showing deformation-induced internal distortion of 5 degrees over a grain size of 250 nm (from Figure 2 of the main text).

**Item DR 3: TKD and TEM Procedure**

Four TKD foils of ca. 15 by 10 μm and 0.1 μm thickness were prepared from the polished thin section used for ESBD analysis using an FEI Nanolab 200 focused ion beam (FIB) instrument. After milling, the foil was cut free, extracted, and placed on a carbon-coated Cu grid. No further carbon coating was necessary.

Transmission Kikuchi diffraction (Trimby, 2012) patterns were collected using a Zeiss Ultra Plus FEG SEM, equipped with an Oxford Instruments Channel 5 EBSD system and a Nordlys-S EBSD detector at the Australian Centre for Microscopy and Microanalysis, The University of Sydney. The TKD signal arises from the lower surface of the foil. TKD analysis was performed at 1-10 nA and 30 kV at high vacuum using a step size of 20 nm. The SEM stage was tilted towards the EBSD detector by 20 degrees at a working distance of typically 5 mm from the pole piece. Processing of TKD data was done in Channel 5 following the same procedure as for EBSD data.

Electron transparent TEM foil samples of thickness ~100 nm were cut perpendicular to the surfaces shown in Figure 2 using a Tescan Lyra FIB-SEM at the Advanced Resource Characterisation Facility located at Curtin University, Perth, Western Australia.

These electron transparent foils were used for the TEM analyses on an FEI Titan G2 TEM/STEM microscope at the University of Western Australia operated at 80 kV and equipped with a Super-X EDS system and a Gatan Enfinium electron energy loss spectroscopy (EELS) detector. A sub-nm probe with a probe current of approximately 0.25 nA was used for STEM image acquisition, EDS and EELS.

Images shown in the manuscript were collected in the bright field TEM and high angle annular dark-field (HAADF) STEM imaging modes showing details of the grains' internal structure and atomic number (Z)-contrast imaging, respectively. EELS spectra were captured by raster scanning a 2 x 20 pixel box covering an area of ~30 x 300 nm (15 nm pixel spacing) acquiring a spectrum with a 1 s acquisition time for each pixel. Analysis of the spectra was carried out using the Gatan software Digital Micrograph where post acquisition treatment of the spectra included alignment and correction of energy drift during spectrum acquisition.

**Item DR 4: Calculation of Frictional Heat Rise during Shearing**

Maximum frictional heating in the gouge is estimated using the model of Rice (2006); accordingly the temperature rise ($\Delta T$) in the slipping zone is calculated as:

$$\Delta T = \frac{\tau_f}{\rho C_p}\sqrt{\frac{Vs}{\pi\kappa}}$$

where $\tau_f$ is the shear strength of the gouge, $\rho$ = density, $C_p$ is the heat capacity, $V$ = slip velocity, $s$ = amount of slip, $\kappa$ = thermal diffusivity.

We used values for heat capacity $C_p$ = 820 J (kg K)$^{-1}$ (Fuchs et al., 2015); density $\rho$ = 2710 kg/m$^3$; and thermal diffusivity of $\kappa = 1.62 \times 10^{-6}$ m$^2$/s (Fuchs et al., 2015). Experimental values of slip velocity $V$ were $2.8 \times 10^{-6}$ m/s and $1.7 \times 10^{-5}$ m/s; while measured shear strength ranged between 37 and 45 MPa. Considering an initial temperature of 25 °C and the values listed above, calculated $\Delta T$ ranges between 4 and 13 °C.

**Item DR 5: EDS and Raman Analysis of Gouge and Identification of Amorphous Carbon**

TEM Energy dispersive X-ray spectroscopy (EDS) was carried out using Bruker's Esprit software by continuously scanning a ~700 x 700 pixel box covering an area of ~ 1 μm x 1 μm (~1.5 nm pixel spacing) using a 100 μs dwell time, acquiring a spectrum at each point in the scan. A total acquisition time of ~30 minutes was used, which ensured good signal-to-noise in the resulting element maps. Spectra were extracted by averaging a small group of pixels from the areas marked in Figure DR5A.

Under EDS investigation, the solid, interstitial material seen between calcite particles that does not yield diffraction patterns in TKD analysis, shows a singular dominance of carbon, not consistent with calcite and interpreted as amorphous carbon (Figure DR5B). EDS based maps reveal that this C-rich phase is interstitial between calcite grains (Figure DR5C)

Raman spectroscopic data were collected on an uncoated petrographic thin section cut normal to the simulated fault and parallel to the sliding direction. Raman spectra were acquired using a Horiba® LabRAM HR Evolution with 600 gr/mm grating, a 532 nm laser produced by a 100mW Quantum Torus continuous wave single frequency diode laser, through a 100x objective (n.a. of 0.90). The detector was a Peltier-cooled Synapse CCD camera and the confocal pinhole reduced to 70. Alteration of the material surface was prevented by decreasing the laser power to 1 mW on the sample surface. The data were collected in the 800-1800 cm-1 range to capture the first order carbon Raman bands. Raman maps were produced on 48 x 40 micrometer area with a step-by-step mapping mode of 0.7 micron XY steps.

In the gouge zone, Raman spectroscopy shows characteristic peaks from co-existing calcite crystals at 1092 $cm^{-1}$ and amorphous carbon with peak at 1617 $cm^{-1}$ (Figure DR5D, E and F).

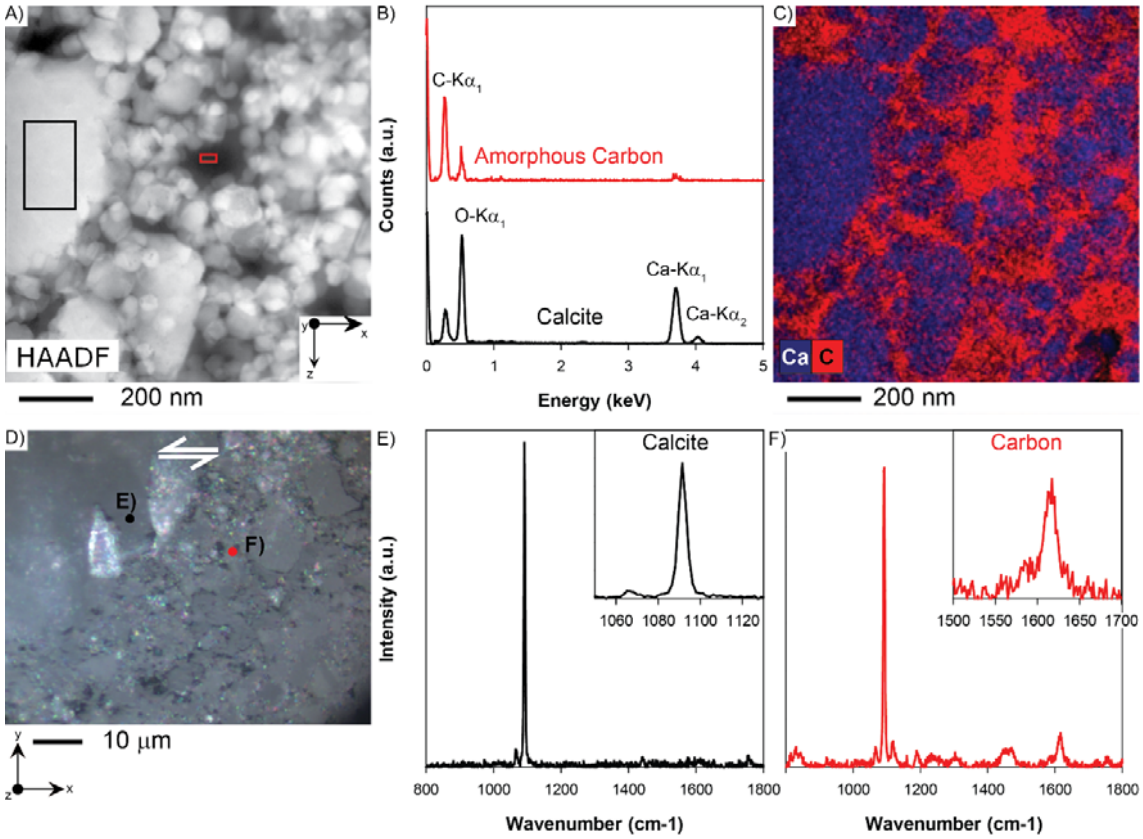


Figure DR5. Chemical characteristics of the calcite gouge. A) HAADF- STEM image of a region of interest characterized by the abundance of sub-micron grains and an interstitial dark phase. B) EDS spectra from the red and black boxes shown in a); black spectrum is for calcite and red spectrum is for amorphous carbon. C) Elemental map showing the distribution of Ca and C as proxies for calcite and amorphous carbon, respectively. D) Reflected light image of a polished surface of an experimentally sheared sample. Raman spectra acquisition locations are indicated as black (E) and red (F) points corresponding to fractured and gouge domains, respectively. E) Raman spectrum of calcite from the fractured domain showing a prominent peak at 1092 $cm^{-1}$ corresponding to the symmetric stretching of the CO3 anion in calcite (Gunasekaran et al., 2006). F) Raman spectrum of co-existing calcite crystals and amorphous carbon with peak at 1617 $cm^{-1}$ ascribed to the D2 band of poorly-ordered carbon (Beyssac et al., 2003) shown in the insert.

**References Cited**


Beyssac, O., Goffé, B., Petitet, J.P., Froigneux, E., Moreau, M. and Rouzaud, J.N., 2003, On the characterization of disordered and heterogeneous carbonaceous materials by Raman spectroscopy: Spectrochimica Acta Part A: Molecular and Biomolecular Spectroscopy, 59(10), pp.2267-2276.

Gunasekaran, S., Anbalagan, G. & Pandi, S., 2006, Raman and infrared spectra of carbonates of calcite structure: Journal of Raman Spectroscopy 37, 892–899.

Marone, C. and Scholz, C. H., 1989 Particle-size distribution and microstructures within simulated fault gouge: Journal of Structural Geology 11, 799–814.

Prior, D.J., Boyle, A.P., Brenker, F., Cheadle, M.C., Day, A., Lopez, G., Peruzzo, L., Potts, G.J., Reddy, S., Spiess, R. and Timms, N.E., 1999, The application of electron backscatter diffraction and orientation contrast imaging in the SEM to textural problems in rocks: American Mineralogist, 84(11-12), pp.1741-1759.

Rice, J. R., 2006, Heating and weakening of faults during earthquake slip: Journal of Geophysical Research: Solid Earth, 111(B5).

Schindelin, J., Arganda-Carreras, I., Frise, E., Kaynig, V., Longair, M., Pietzsch, T., Preibisch, S., Rueden, C., Saalfeld, S., Schmid, B. and Tinevez, J.Y., 2012, Fiji: an open-source platform for biological-image analysis: Nature methods, 9(7), pp.676-682.

Fuchs, S., Balling, N. and Förster, A., 2015. Calculation of thermal conductivity, thermal diffusivity and specific heat capacity of sedimentary rocks using petrophysical well logs. Geophysical Supplements to the Monthly Notices of the Royal Astronomical Society, 203(3), pp.1977-2000.

Timms, N. E., Li, J. and Reddy, S. M., 2009, Quantitative microstructural characterization of natrojarosite scale formed during high-pressure acid leaching of lateritic nickel ore: Am. Mineral. 94, 1111.

Trimby, P.W., 2012, Orientation mapping of nanostructured materials using transmission Kikuchi diffraction in the scanning electron microscope: Ultramicroscopy, 120, pp.16-24